Photoluminescence study of non-polar m-plane InGaN and nearly strain-balanced InGaN/AlGaN superlattices

Yang Cao,[1] Brandon Dzuba,[1,2] Brenden A. Magill,[3] Alexander Senichev,[1,2] Trang Nguyen,[1] R. E. Diaz,[2] Michael J. Manfra,[1,2,4,5] Stephen McGill,[6] Carlos Garcia,[6] Giti A. Khodaparast,[3] Oana Malis[1,*]

[1]*Department of Physics and Astronomy, Purdue University, West Lafayette, IN 47907, USA*

[2]*Birck Nanotechnology Center, West Lafayette, IN 47907, USA*

[3]*Department of Physics, Virginia Tech, Blacksburg, VA, 24061, USA*

[4]*School of Electrical and Computer Engineering, Purdue University, West Lafayette, IN 47907, USA*

[5]*School of Materials Engineering, Purdue University, West Lafayette, IN 47907, USA*

[6] *National High Magnetic Field Laboratory, Tallahassee, FL 32310, USA*

Abstract

Photoluminescence (PL) spectroscopy of nonpolar m-plane InGaN thin films with indium composition up to 21% and nearly strain-balanced $In_{0.09}Ga_{0.91}N/Al_{0.19}Ga_{0.81}N$ superlattices grown by plasma-assisted molecular beam epitaxy was performed as a function of temperature. The experimental transition energies are consistently lower than the calculation based on structural parameters extracted from x-ray diffraction measurements. This indicates the presence of indium-composition fluctuations in InGaN and hence local band gap reduction that produces charge localization centers. The spectral width of the low-temperature PL of our m-plane InGaN/AlGaN superlattices is narrower than previously reported for m-plane InGaN/GaN quantum wells grown by MOCVD. The PL integrated intensity drops rapidly, though, as the temperature is increased to 300 K indicating strong non-radiative recombination at room temperature. Time-resolved PL at low temperatures was performed to characterize the relaxation time scales in an undoped as well as a doped superlattice.

[*] Author to whom correspondence should be addressed. Electronic mail: omalis@purdue.edu

1. Introduction

III-nitride semiconductors have sustained remarkable practical interest over the last two decades due to their large band gap range (0.7 eV to 6.2 eV), and large conduction band offsets. This combination of properties makes it possible to design III-nitride optoelectronic devices operating at wavelengths from ultra-violet to far-infrared.[1] Furthermore, the superior electron mobility, thermal and chemical stability, thermal conductivity, breakdown voltage, and saturated drift velocity of nitrides also found applications in various electronic devices.[2-3] Much research has been done on polar c-plane III-nitride heterostructures to date, but the existence of internal polarization fields restricts the design of certain devices, especially for infrared applications.[4-9] Since non-polar m-plane structures eliminate the internal polarization fields, they have attracted significant attention recently. In particular, nonpolar nitride infrared devices have the potential to exceed the spectral range and performance of their polar counterparts, and of any other material system.[10-11]

This paper presents the results of a systematic photoluminescence (PL) study for non-polar m-plane InGaN thin films and nearly strain-balanced InGaN/AlGaN superlattices grown by plasma-assisted molecular-beam epitaxy (MBE). The InGaN thin films were selected to examine the effect of In-composition alone on the optical properties. The superlattices were designed primarily to increase the conduction-band offset between the InGaN quantum wells (QW) and AlGaN barriers for applications in novel near-infrared intersubband devices.[1,4,5] While the PL characterizations of c-plane InGaN thin layers and quantum wells have been reported extensively, there are much fewer published studies of m-plane InGaN. Moreover, most of the published PL investigations of m-plane InGaN to date were done on structures grown by metal-organic chemical-vapor deposition (MOCVD).[12-20] For instance, Sutherland *et al.* studied m-plane InGaN/GaN QWs grown by MOCVD and found their quantum efficiency to be lower than the efficiency of similar c-plane structures.[12] The reason for this lower efficiency is not completely understood at this point, and it is likely due to defects specific to the m-plane heterostructures.

Although significant progress has been made towards improving the growth of non-polar nitride materials, the structural quality of m-plane materials still lags behind the quality of c-plane nitride heterostructures. This is primarily due to the challenges involved in epitaxial growth on the m-plane surface.[21-26] A distinct challenge of m-plane growth is the adatom mobility difference between the c- and the a-direction that results in different growth dynamics, and ultimately different growth conditions, for the m-plane as compared to the isotropic c-plane surface. Another challenge for m-plane nitride heterostructures is the anisotropic lattice-mismatch between GaN, InGaN, and

AlGaN. Strain buildup in lattice-mismatched materials leads to extended defects and eventually to macroscopic cracks. For example, strain can lead to pronounced alloy inhomogeneity and interface roughness for Al-compositions above 50%.[24] Therefore, to minimize AlGaN inhomogeneity and mitigate strain buildup in thick In-containing nitrides, this study investigates nearly strain-balanced $In_{0.09}Ga_{0.91}N/Al_{0.19}Ga_{0.81}N$ superlattices.

2. Experimental and calculation details

Our samples were grown by plasma-assisted MBE on commercially available non-polar m-plane $(10\bar{1}0)$ semi-insulating GaN substrates from Nanowin, Inc. The root-mean-square roughness of the substrates is less than 0.3nm over 16 μm^2, measured by atomic force microscopy (AFM). The nominal threading dislocation density is less than 5×10^6 cm^{-2}. The substrates are miscut $-0.5^o \pm 0.2^o$ towards the c-axis. The size of the substrates is about 5×10 mm^2. The details of the growth are given elsewhere.[25] Briefly, the substrates were mounted on 2 inch c-plane GaN-on-sapphire wafers. Our MBE system is equipped with conventional effusion cells for indium, gallium, and aluminum. The active nitrogen flux was supplied by a Veeco Unibulb radio-frequency plasma source operated at 300W forward power with 0.5 sccm of nitrogen (N_2) flow. A GaN buffer layer was first grown at 720°C. The growth temperature of the In-containing materials was adjusted in the range of 450°C-635 °C to obtain different In compositions. An effusion cell was used to provide silicon for delta-doping in the superlattice barriers.

High-resolution x-ray diffraction (HRXRD) was used to characterize the structure of our samples. ω-2θ spectra and reciprocal-space maps were collected by a PANalytical X'Pert-MRD high-resolution x-ray diffractometer equipped with a 4-bounce Ge monochromator. The software package Epitaxy 4.5a from PANalytical was used to simulate the HRXRD diffraction patterns in order to extract layer thicknesses and alloy compositions. The InGaN thin layers have a thickness of approximately 30 nm and the alloy compositions given in Table I below. The superlattice structural parameters are given in the Table II below. The HRXRD structural information was confirmed and supplemented with scanning transmission electron microscopy (STEM) data. Samples for STEM were prepared using focus ion beam (FIB) *in situ* lift-out technique performed using a Thermo Scientific Helios G4 UX Dual Beam instrument. The process was ended with a polishing procedure at 500 V and 48 pA with the ion beam to further thin down the specimen and reduce the areas damaged by the high energy ion beam. Before loading into the microscope column, each sample was cleaned with a Fischione Ar plasma cleaner for 1 hour to reduce possible specimen

contamination. STEM images were taken with an Aberration Corrected Themo Scientific Themis Z at 300kV and 0.23nA.

For continuous excitation PL experiments, the samples were placed in a liquid He flow cryostat and measured in reflection geometry in the range from 8 K to room temperature. Excitation power of about 10 mW (estimted cw photo-excited carrier density is 6.3×10^{11}cm^{-3}) was provided by a 325 nm cw He-Cd laser. The PL spectra were recorded with a Cary Eclipse Fluorescence Spectrometer equipped with a photomultiplier tube. To extract the transition energy and full-width-at-half-maximum (FWHM), the spectra were corrected by subtracting a linear background and fit with a Lorenzian function. The integrated intensity was obtained by numerical integration over the measured energy range.

The band gap of relaxed InGaN was calculated by the following formula:[27,28]

$$E_{In_xGa_{1-x}N} = xE_{InN} + (1-x)E_{GaN} - bx(1-x), \quad (1)$$

where the bowing parameter, b, was taken to be 1.43eV.[27] The temperature dependence of the band gaps is given by the Varshni relation:[29]

$$E_g(T) = E_g(0) - \frac{\alpha T^2}{T+\beta} \quad (2)$$

where $E_g(0)$ is the band gap at 0K. $E_g(0) = 3.51\,\mathrm{eV}$, $\alpha = 0.909\,\mathrm{meV/K}$, $\beta = 830\,\mathrm{K}$, and $E_g(0) = 0.78\,\mathrm{eV}$, $\alpha = 0.245\,\mathrm{meV/K}$, $\beta = 624\,\mathrm{K}$, are recommended by Vurgaftman *et al.* for GaN and InN, respectively.[28] We used the nextnano software package for the self-consistent simulation of the band structures of strained InGaN layers and InGaN/AlGaN superlattices.[30]

Since the measured PL is likely due to excitons, the calculated transition energies were also corrected to include the exciton binding energy. The energy shift due to this effect is expected to be less than 60meV.[14] The exact value of this energy shift is hard to calculate, but we used the simple hydrogen atom-like model to estimate it. Therefore, the excitonic binding energy was calculated using

$$E_X = \frac{m_r R_y(\mathrm{H})}{m_0 \varepsilon^2}.$$

Where m_0 is the free-electron mass, and m_r is the reduced mass of the effective masses of electron and hole in the exciton. $R_y(\mathrm{H}) \approx 13.6\mathrm{eV}$ is the Rydberg energy. $m_r \approx 0.17\ m_0$,[28] and $\varepsilon \approx 10$.[31]

Time-resolved photoluminescence (TRPL) was measured in a Helium flow-thru cryostat from 2 K to 100 K temperature range. A Mira 900 Ti:sapphire oscillator with a repetition rate of 80 MHz was provided 784 nm pulses which were upconverted to 384 nm using a non-linear crystal (BBO) then used to excite the samples (photo-induced density of ~ 4.8×10^{14} cm^{-3}). Light emitted at the PL peak (~408 nm) was selected using a monochrometer then collected from the sample in a reflectivity geometry using an avalanche photodiode. A time correlated single photon counting system (Picoharp 300) was used to determine the time between excitation pulse and emission of PL photons.

3. Results and Discussion

3.1 Photoluminescence of m-plane InGaN layers

To study the dependence of photoluminescence on the In-composition, we first discuss the results for a series of 30-nm InGaN thin layers grown at different substrate temperatures to vary the In incorporation.[25] The structural information of the measured samples is listed in Table I. Table I also provides a summary of our PL results at 80 K, as well as the calculated peak positions, corresponding to HRXRD compositions including exciton binding energy correction for relaxed and coherently strained InGaN on GaN. The PL spectra of samples A-D at 80 K are shown in Figure 1. The PL intensity decreases rapidly with increasing the In composition for samples B-D, but to the best of our knowledge, this is the first report of PL measurements in m-plane InGaN structures grown by MBE with average composition up to 21%. We note, however, that the PL intensity of sample B (11%) is larger than that of sample A (6.4%). We attribute this effect to improved material quality of sample B due to optimal MBE conditions, as indicated by the narrower linewidth.

Table I. The PL results at 80 K for a series of InGaN thin layers with different In compositions, and the corresponding calculated peak energies for relaxed InGaN layers as well as films coherently strained to GaN substrates.

Sample #	In composition (HRXRD)	Exp. peak position (eV)	Exp. FWHM (nm) (meV)	Cal. peak position relaxed InGaN (eV)	Cal. peak position strained InGaN (eV)	Estimated In composition of strained InGaN from exp. PL
A	6.4%	3.131	68	3.217	3.280	11%
B	11.0%	3.002	53	3.037	3.137	15%
C	16.2%	2.756	83	2.842	2.979	24%
D	21.0%	2.637	93	2.668	2.836	28%

We found the PL peak energy of m-plane InGaN films to be systematically smaller than the theoretical energy calculated using the nominal In composition from HRXRD. This difference is particularly large (up to 0.2 eV), if we consider the InGaN films to be coherently strained to the GaN layer. We note that HRXRD reciprocal space mapping indicated that all films up to 21% are coherently strained on the m-plane GaN substrate.[25] The last column of Table I shows the In composition estimated from the experimental peak position assuming strained films. The difference in In-composition between estimated and measured values varies between 4-7%. Possible reasons for this discrepancy include the uncertainty of structural parameters in the HRXRD simulation, and the uncertainty of deformation potentials in the nextnano simulation. However, a more likely explanation of this discrepancy is the inhomogeneous In distribution of InGaN.[14] The HRXRD-extracted composition is an average over the entire film, while the PL transition energy reflects the bandgap minimum given by the alloy fluctuations with maximum In composition. Therefore, we believe that the m-plane InGaN alloy may have composition fluctuations of up to 7% for the largest In composition films (21%).

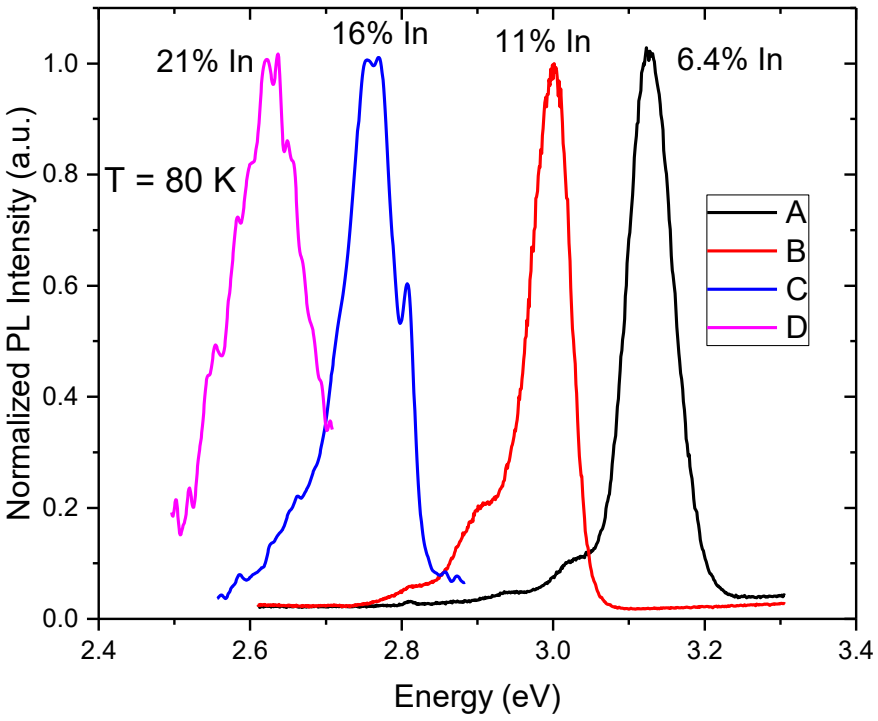

Figure 1. The PL spectra of the samples with 30 nm thick layer of our InGaN with different compositions (samples A-D) at 80 K. The spectra were normalized to their respective maximum. The spectra for samples A-D were reduced by a factor of 545, 1000, 17.8, and 8.5, respectively.

At 80 K, the FWHM of the m-plane InGaN samples B-D increases with the In composition. We note that sample A doesn't seem to follow this trend. However, we believe that the differences between samples A and B are due to material quality properties beyond our control. The relation between the FWHM of the PL spectrum and the alloy composition's distribution can be calculated theoretically assuming a random alloy structure with a binomial In distribution.[32-33] This model excludes any alloy inhomogeneities in the lateral or growth direction, as well as other broadening mechanisms due to defects, alloy clustering, etc.

Therefore, the calculations provide only a rough guidance for the minimal theoretical linewidth of an ideal alloy semiconductor. We observed linewidths for sample A (6.4% In) and sample B (11%In) (68, and 53 meV, respectively) that are larger than the theoretical estimates (35 meV and 42 meV, for 7% and 11%, respectively), but comparable to the measured c-plane values. It has been reported that some c-plane InGaN thin layers have 3-4 times broader FWHM than the calculations.[34-36] The FWHM of our 16% In sample C (83 meV) is a factor of two larger than the maximum theoretical value, but only slightly larger than the measured quantities for the c-plane InGaN/GaN quantum wells with similar In composition (~74 meV).[36]

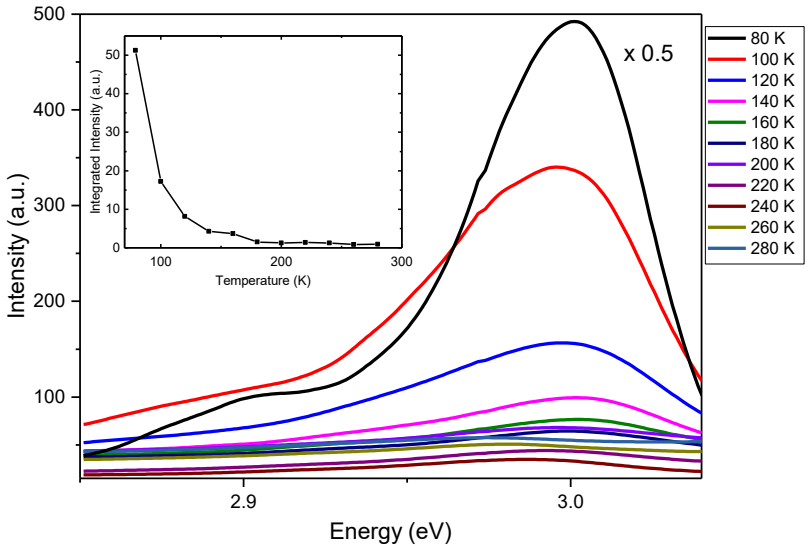

Figure 2. The temperature dependence of the PL spectra for 30 nm thick $In_{0.11}Ga_{0.89}N$ film (sample B). Inset: the temperature dependence of the integrated PL intensity of sample B.

Figure. 2 shows the temperature dependence of the spectra for sample B. At low temperature, the spectra show one or two small peaks on the low energy side of the main peak due to longitudinal-optical phonon assisted

emission. We found the PL intensity decreases drastically as temperature increases. The inset shows the temperature dependence of integrated PL intensity for sample B. Since the internal quantum efficiency (IQE) is related to the integrated PL intensity,[37] the IQE drops significantly for our InGaN thin layers at room temperature. Moreover, the temperature dependence of the peak position for sample B can be seen in Fig. 3(a). The curve is not monotonic and does not follow the behavior expected for the temperature dependence of the bandgap. A similar phenomenon was previously reported for c-plane InGaN thin layers (commonly referred to as "S-shape" curve)[36,38] and was attributed to carrier localization centers in InGaN. As temperature increases, the active charges may stay in the original localization centers, become delocalized, or get trapped in different centers. Once the charge configuration changes, the PL peak position may also change in an uncontrolled manner. Furthermore, the temperature dependence of the peak position may vary with the In composition, since the properties of localized centers likely change with composition.

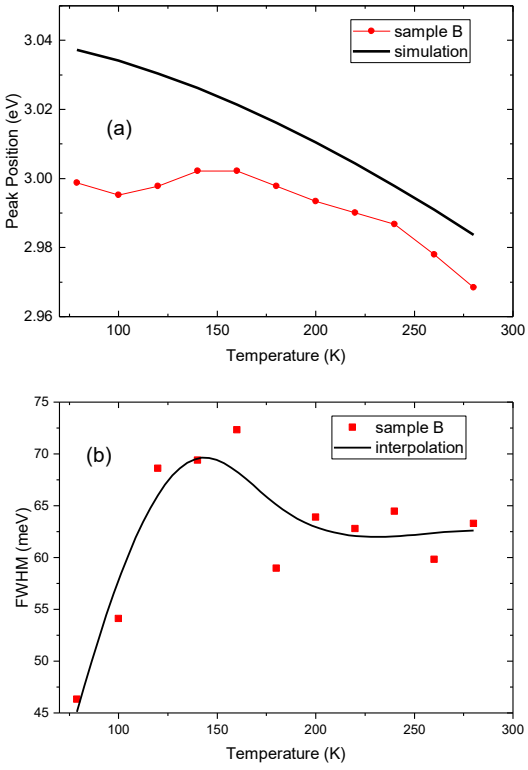

Figure 3. (a) The temperature dependence of the PL peak positions for the $In_{0.11}Ga_{0.89}N$ 30 nm thin film (sample B) compared to the theoretical prediction (black line) of the temperature bandgap dependence for a relaxed film. (b) Temperature dependence of the FWHM of sample B. The black line is just a guide to the eye.

In the absence of previous studies related to the temperature dependence of PL in the m-plane InGaN thin layers grown by MBE, we compare our data with results for the c-plane InGaN grown by MOCVD. We found that our m-plane InGaN films exhibit very weak PL at room temperature, in contrast with the c-plane InGaN films of similar composition that exhibit PL, all the way to room temperature.[37] We attribute the large difference of the PL intensity between the m-plane and c-plane InGaN thin layers in part to the differences in the band structure. In c-plane InGaN, the internal polarization causes band tilting that enhances charge localization, and consequently PL intensity. On the other hand, the growth processes for the m-plane InGaN thin layers may result in incorporation of more non-radiative recombination centers, especially for the samples with high In composition, which lower the PL signal. Lastly, the temperature dependence of the FWHM (Fig. 3(b)) is comparable to that reported for the c-plane InGaN films of similar composition grown by MOCVD.[35]

3.2 Photoluminescence of strain-balanced m-plane InGaN/AlGaN superlattices

Relatively limited studies have been reported on the growth of strain-balanced m-plane InGaN/AlGaN superlattices[39] and their PL characterization.[20] Table II shows the summary of the structural information and our PL results for a series of InGaN/AlGaN superlattices. The superlattices nominally consist of 15 InGaN quantum wells (QWs) (the In composition approx. 9%) separated by $Al_{0.19}Ga_{0.81}N$ barriers. The barrier composition was chosen low enough to minimize the interface roughness and the alloy inhomogeneity. Moreover, the barrier thickness was selected so that the tensile strain of the AlGaN barriers approximately balances the compressive strain of the QWs. The resulting superlattice period is approximately strain-balanced along the a-direction with a residual tensile strain of less than 0.3% along the c-direction. Careful examination of STEM (Fig. 4(b)) revealed no dislocation formation. However, STEM identified the presence of an unintentional ~1.3 nm GaN layer on top of each barrier (shown schematically in Fig. 4(a)) formed due to excess Ga accumulation during the barrier growth and the preferential incorporation in the QW. Therefore, the calculation of the transition energies in Table II was done using this additional GaN layer. Some of the structures were doped with two delta-doping sheets of silicon, placed in the barriers, 1 nm away from each interface, as indicated in Fig. 4(a). The doping level is specified in Table II by the deposition time of a single delta-doping sheet. Silicon deposition of 10-seconds corresponds to a dopant density of about 2×10^{14} cm^{-2}.

Table II. The structural parameters and summary of our PL results at 80 K for a series of nearly strain-balanced m-plane InGaN/AlGaN superlattices (samples G-J). For reference, the PL results for an m-plane GaN/AlGaN superlattice are also provided (sample F).

#	In/Al composition	QW thickness /barrier (nm)	δ-doping	Exp. peak position (eV)	Cal. peak position (eV)	Exp. FWHM (meV)
F	0/16.5%	3/3.3	undoped	3.53	3.570	70
G	9.0%/18.8%	3.15/6.4	undoped	3.07	3.314	73
H	8.7%/18.8%	2.95/6.4	10sec	3.06	3.319	117
J	9.3%/18.8%	2.95/6.4	20sec	3.07	3.300	172

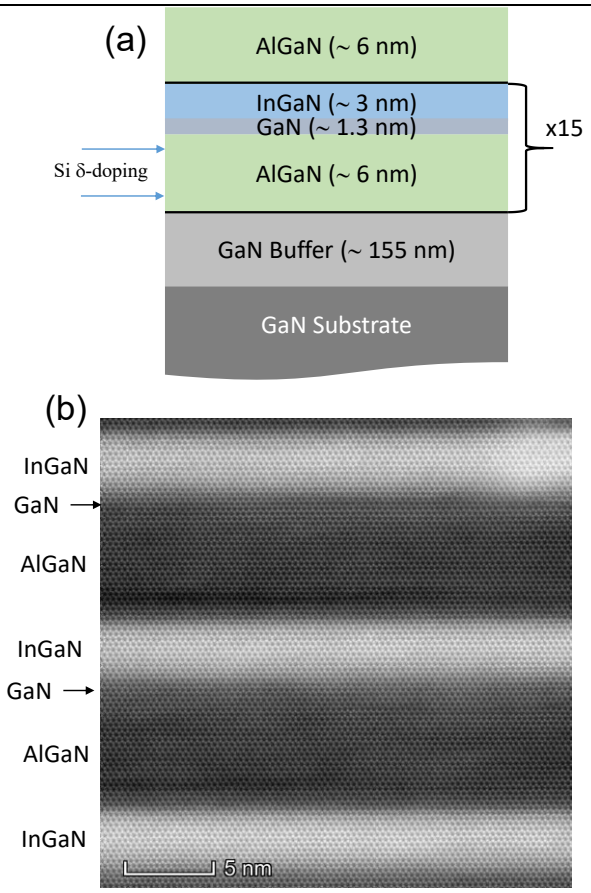

Figure 4. (a) The sketch of the structure for the superlattices G-J. (b) The STEM of the superlattice with the structure of sample J. The lighter layers are the InGaN while the darker layers are the AlGaN.

Even after considering that the GaN layers are unintentionally deposited on the top of the barriers, we found a significant discrepancy between the calculated and the measured PL peak energies of InGaN/AlGaN superlattices. This discrepancy is larger than the scenario described earlier for the thin InGaN strained films (e.g. the sample B). For reference, Table II also includes the results for a strained GaN/AlGaN superlattice (sample F). The PL peak energy of

the sample F is also lower than the calculated value, but the difference between these two values is of the same magnitude as for the thin InGaN films. This indicates that the discrepancy between experiment and calculations for the InGaN/AlGaN superlattices originates in the InGaN layer.

The most natural explanation of the difference between the experiment and calculations can be related to the presence of the In composition fluctuations. As mentioned above, we already have evidence for these fluctuations extracted from the PL response of the thin InGaN layers. The quantum confinement in the QWs likely enhances the effect of these fluctuations, further increasing the difference between the calculated and the measured transition energies. The measured PL energy corresponds to an average In-composition of ~17% in the InGaN QWs. Therefore, the QWs must have In-rich regions with at least this composition. As stated earlier, a possible alternative explanation for the difference between the calculation and the measurements could be due to an overestimation of the strain (larger bandgap) for the bandgap of InGaN, i.e. inaccuracies of deformation potentials in the calculations. We note that polarized PL measurements at 80K were also performed and the degree of optical linear polarization was found to be 83% preferentially perpendicular to the c-axis. This result agrees with previous reports,[45-47] and indicates that the films are bi-axially strained, as expected from x-ray reciprocal-space mapping.[25]

We also measured the temperature dependence of the PL spectra for these superlattices, as shown in Fig. 5. The PL integrated intensity drops dramatically when temperature is increased to 300 K (inset of Fig. 5). This indicates the presence of non-radiative recombination centers with densities larger than previously reported for m-plane InGaN/GaN QWs grown by MOCVD.[12-20] These additional non-radiative recombination centers are likely due to the lower growth temperature in MBE than in MOCVD.

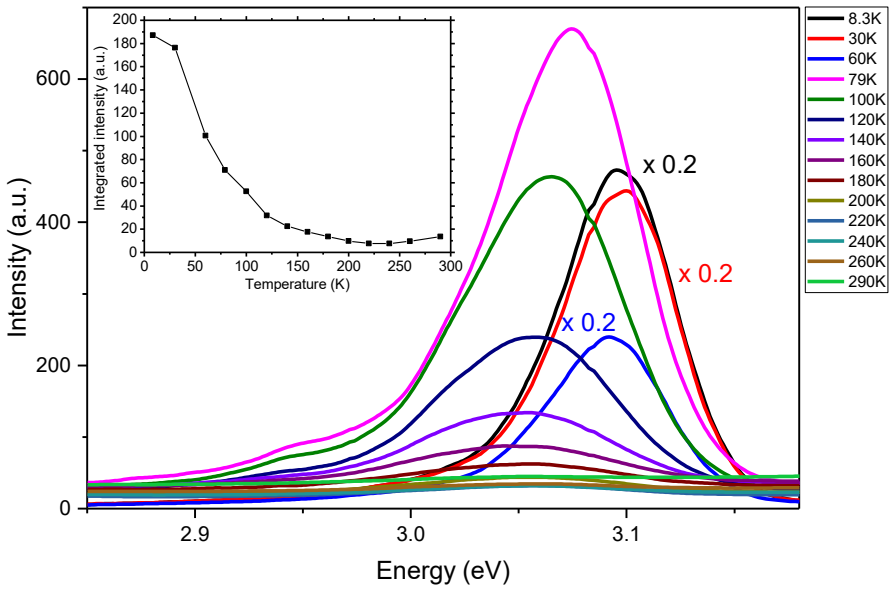

Figure 5. The temperature dependence of the PL spectra for InGaN/AlGaN undoped superlattice, sample G. Inset: temperature dependence of integrated PL intensity of sample G.

Figure 6 shows the temperature dependence of peak position and FWHM for sample G. This dependence is non-monotonic (Fig. 6a), consistent with that observed for the InGaN thin layers, and is also likely due to exciton localization in the high-indium regions of the QWs. The FWHM of sample G increases with temperature as expected (Fig. 6b). However, the low temperature FWHM of the undoped sample G is approximately equal to that of sample F, suggesting similar inhomogeneous broadening mechanisms for the GaN/AlGaN and InGaN/AlGaN superlattices. Moreover, the FWHM of sample G is only slightly larger than that of the thin InGaN films of comparable composition (samples A and B). The excess broadening of the superlattice PL peak relative to the thin film PL is likely due to the QW interface roughness.[40] Furthermore, the low-temperature FWHM of sample G is narrower than some values reported in the literature for m-plane InGaN/GaN QWs. For instance, a 5-period m-plane $In_{0.14}Ga_{0.86}N$/GaN superlattice grown by MOCVD was reported to have a PL peak at 408 nm (3.038 eV) with the peak width of 14.92 nm (121 meV) at 10 K.[13] Therefore, our low-temperature PL results for MBE-grown m-plane InGaN/AlGaN superlattices compare favorably to previous published results for MOCVD-grown InGaN/GaN superlattices.[12-15]

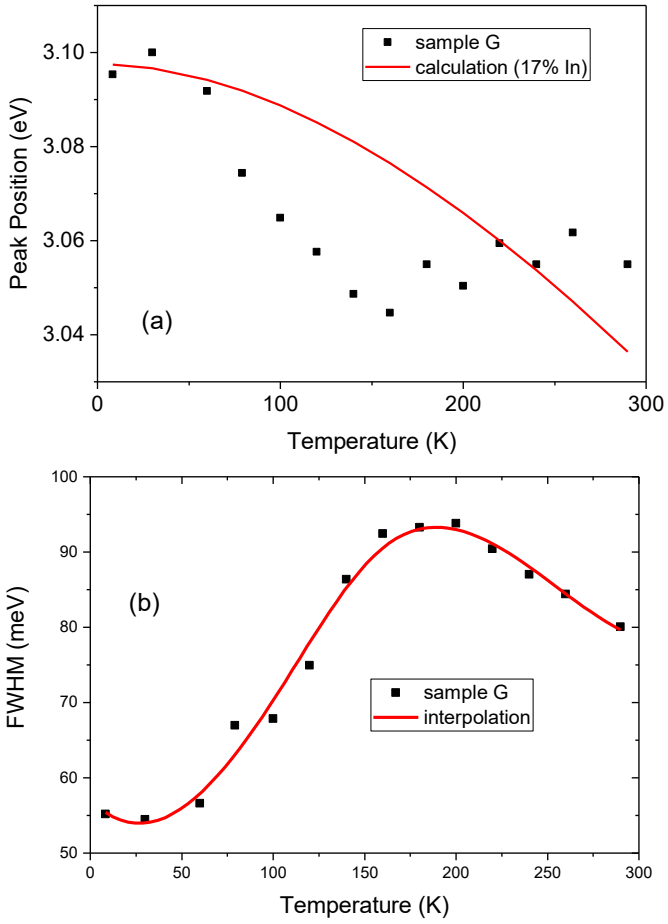

Figure 6. The temperature dependence of the PL peak positions. (a), and FWHM (b) for the InGaN/AlGaN undoped superlattice sample G. The red line in (a) is the calculation of the PL energy for a superlattice with the $In_{0.17}Ga_{0.83}N$ QWs. The red line in (b) is just a guide to the eye.

Intentional doping in the barriers increases the peak width significantly. Comparing our samples G and H, we found that two 10-second δ-doping sheets in the barriers increase the FWHM from 73 to 117 meV. Moreover, sample J has twice of the δ-doping compared to the sample H, and considerably larger peak width (172 meV). We speculate that the additional inhomogeneous broadening may be due to impurity and electron-electron scattering that increase rapidly with doping density. Unlike the case of c-plane QWs, the effect of doping on barrier band tilt[41] is expected to be minor for m-plane structures. However, additional alloy inhomogeneity and surface roughness, induced by the Si dopant incorporation cannot be excluded as possible sources for the broadening.[48] Identifying the exact cause of this broadening is of practical interest for devices and will be pursued in our future studies.

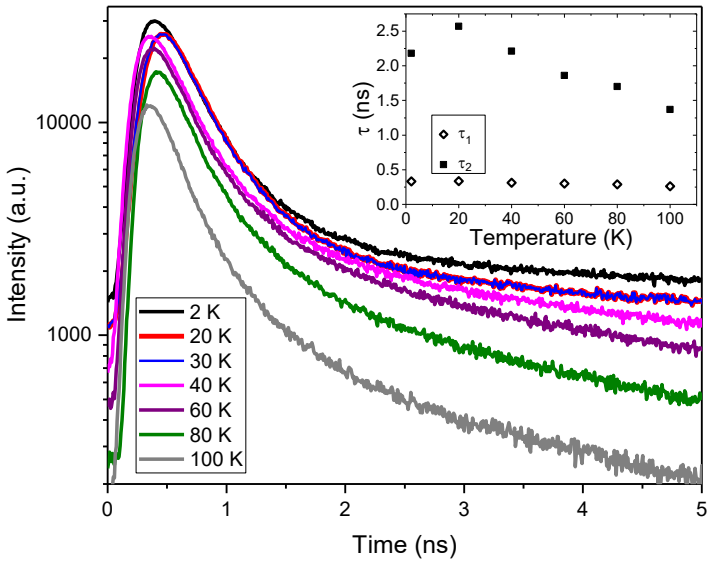

Figure 7. Our TRPL of the undoped InGaN/AlGaN superlattice (sample G) was measured for the emission near the PL peak (414 nm), using a 384 nm excitation with 80 μW average power, for temperatures between 2 and 100 K. The inset presents the relaxation time constants τ_1 and τ_2 as a function of temperature.

3.3 Time resolved photoluminescence of strain-balanced InGaN/AlGaN superlattices

Figure 7 shows the TRPL of the undoped InGaN/AlGaN superlattice, the sample G. The time scales of the observed dynamics were described by two time constants τ_1 and τ_2. This fact suggests that excitons relax through two channels. The time scale of the fast decay, τ_1, is ~ 0.3 ns, with the slower one, τ_2, approximately 1 ns. Both time constants decrease with increasing temperature, but the change of τ_2 is more dramatic (a factor > 1.5) over the measured temperature range. We observed the bi-exponential decay pattern over all the temperature range in this measurement (2-100 K), but it could still be reasonable to attribute the observed time scale (τ_1) in sample G to Shockley-Read-Hall (SRH) and the longer time scale to radiative decay, similar to what has been reported by earlier studies.[49,50] The slow decay component could also be the consequence of a long multistep relaxation process involving carrier cooling through LO-phonon emission.[42]

The estimated τ_1 here is similar to the values reported for m-plane InGaN/GaN quantum wells grown by MOCVD.[12,13,15,18,44,48] A longer time constant has also been reported before and was attributed to the QW on semipolar facets formed due to step bunching during growth.[12] While we cannot completely exclude the possibility of semipolar

facet formation in our samples, we found no evidence for them in the STEM images. Another possible cause of the longer time constant is the presence of the in-plane piezoelectric fields due to dislocations.[43] Nevertheless, both time constants are much shorter than the measured values in the c-plane QWs, indicating faster recombination in nonpolar m-plane structures than in c-plane structures,[50,51] in agreement with previous publications.[52] However, further research will need to be done to determine whether this is due to an increase in radiative recombination, or to an increase in point defects.

Figure 8 shows the TRPL of doped InGaN/AlGaN superlattice (sample H). In this case, the PL dynamics can be characterized by a single time constant τ_1 (~ 0.3 ns) at low temperatures, which decreases moderately with increasing temperature. The origin of this single decay channel is not known at this time and deserves further investigation.

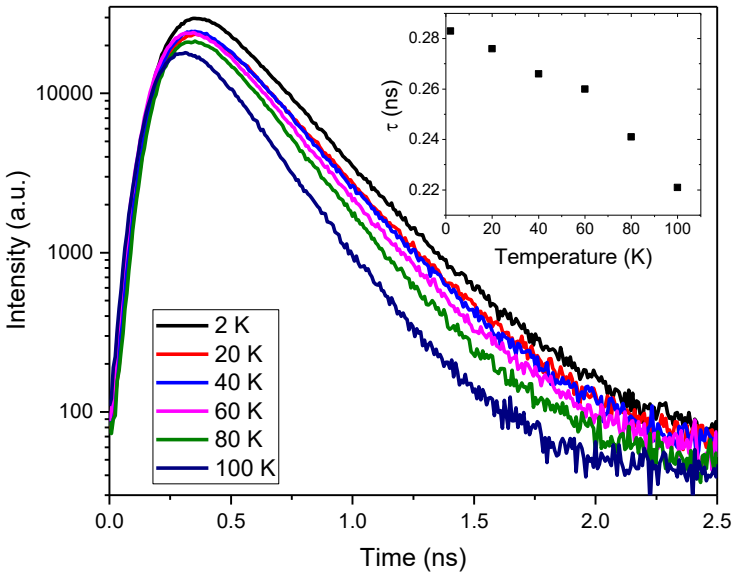

Figure 8. The TRPL of the doped InGaN/AlGaN superlattice (sample H) was measured for emission near the PL peak (414 nm), using a 384 nm excitation with the average power of 80 μW, for temperatures between 2 and 100 K. We plotted the log of the intensity as a function of time. The inset presents τ_1 as a function of temperature.

4. Conclusion

In conclusion, photoluminescence spectroscopy was employed to characterize the optical properties of nonpolar m-plane $In_xGa_{1-x}N$ ($x \leq 0.21$) thin films and strain-balanced $In_xGa_{1-x}N/Al_yGa_{1-y}N$ ($x = 0.09$, $y = 0.19$) superlattices grown by plasma-assisted MBE. In spite of the relatively low growth temperature needed for significant indium incorporation in MBE, the optical properties of the materials are equivalent to those reported in the literature for m-plane InGaN/GaN superlattices grown by MOCVD. Both types of our samples exhibit strong PL at low temperatures that decreases rapidly when the temperature is increased to 300 K. The PL energy is consistently lower than calculated using the HRXRD composition and the recommended band structure parameters.[28] The PL energies and the temperature dependence of the peak positions indicate the presence of indium fluctuations as high as 7% above nominal composition that act as charge localization centers. However, we note that the magnitude of these fluctuations would be smaller if the generally accepted deformation potentials overestimate the effect of strain on InGaN bandgap. The inhomogeneous broadening of low-temperature PL of our m-plane InGaN/AlGaN undoped superlattice is smaller than recently reported for m-plane InGaN/GaN quantum wells grown by MOCVD.[12-15] Our time-resolved PL spectroscopy of two superlattices indicates significantly different relaxation dynamics in the doped and undoped superlattices.

Acknowledgments

We acknowledge support from the National Science Foundation. YC, TN, and OM acknowledge partial support from NSF grant NSF award DMR-1610893. AS and BD were supported from NSF award ECCS-1607173.

GAK and BAM acknowledge the support from AFOSR under Grant FA9550-17-1-0341. A portion of this work was performed at the National High Magnetic Field Laboratory, which is supported by the National Science Foundation Cooperative Agreement No. DMR-1157490 and the State of Florida.

References

[1] T. D. Moustakas, and P. Paiella*, Rep. Prog. Phys.* **80**, 106501 (2017).

[2] C. Zhou, A. Ghods, V. G. Saravade, P. V. Patel, K. L. Yunghans, C. Ferguson, Y. Feng, B. Kucukgok, N. Lu, and I. T. Ferguson, *ECS J. Solid State Sci. Technol.* **6**, Q149–Q156 (2017).

[3] H. Morkoc, S. Strite, G. B. Gao, M. E. Lin, B. Sverdlov, and M. Burns, *J. Appl. Phys.* **76**, 1363–1398, (1994).

[4] M. Beeler, E. Trichas and E. Monroy, *Semicond. Sci. Technol.* **28**, 074022 (2013).

[5] J. Wu, *J. Appl. Phys.* 106, 011101 (2009).

[6] O. Malis, C. Edmunds, M. J. Manfra and D. L. Sivco, *Appl. Phys. Lett.* **94**, 161111 (2009).

[7] C. Edmunds, L. Tang, D. Li, M. Cervantes, G. Gardner, T. Paskova, M. J. Manfra, and O. Malis, *J Electr Mater.* **41**, 881 (2012).

[8] C. Edmunds, L. Tang, J. Shao, D. Li, M. Cervantes, G. Gardner, D. N. Zakharov, M. J. Manfra, and O. Malis, *Appl. Phys. Lett.* **101**, 102104 (2012).

[9] C. Edmunds, L. Tang, M. Cervantes, M. Shirazi-HD, J. Shao,A. Grier, A. Valavanis, J. D. Cooper, D. Li, G. Gardner, D. N. Zakharov, Z. Ikonic, D. Indjin, P. Harrison, M. J. Manfra, and O. Malis, *Phys. Rev. B* **88**, 235306 (2013).

[10] C. Edmunds, J. Shao, M. Shirazi-HD, M. Manfra, and O. Malis, *Appl. Phys. Lett.* **105**, 021109 (2014).

[11] D. Feezell, Y. Sharma, and S. Krishna, *J. Appl. Phys.* **113**, 1133103 (2013).

[12] D. Sutherland, T. Zhu, J. T. Griths, F. Tang, P. Dawson, D. Kundys, F. Oehler, M. J. Kappers, C. J. Humphreys, and R. A. Oliver, *Phys. Status Solidi (b)* **252**, 965-970 (2015).

[13] D. Kundys, D. Sutherland, M. J. Davies, F. Oehler, J. Griths, P. Dawson, M. J. Kappers, C. J. Humphreys, S. Schulz, F. Tang, and R. A. Oliver, *Sci. Technol. Adv. Mater.* **17**, 736-743 (2016).

[14] S. Schulz, D. P. Tanner, E. P. O'Reilly, M. A. Caro, T. L. Martin, P. A. J. Bagot, M. P. Moody, F. Tang, J. T. Griths, F. Oehler, M. J. Kappers, R. A. Oliver, C. J. Humphreys, D. Sutherland, M. J. Davies, and P. Dawson, *Phys. Rev. B.* **92**, 235419 (2015).

[15] S. Marcinkeviius, K. M. Kelchner, S. Nakamura, S. P. DenBaars, and J. S. Speck, *Phys. Status Solidi (c)* **11**, 690-693 (2014).

[16] K. M. Kelchner, L. Y. Kuritzky, K. Fujito, S. Nakamura, S. P. DenBaars, and J. S. Speck, *J. Cryst. Growth.* **382** 80-86 (2013).

[17] M. Sawicka, P. Wolny, M. Kryko, H. Turski, K. Szkudlarek, S. Grzanka, and C. Skierbiszewski, *J. Cryst. Growth.* **465** 43-47 (2017).

[18] P. Dawson, S. Schulz, R. A. Oliver, M. J. Kappers, and C. J. Humphreys, *J. Appl. Phys.* **119**, 181505 (2016).

[19] S. Kusanagi, Y. Kanitani, Y. Kudo, K. Tasai, A. A. Yamaguchi, and S. Tomiya, *Jap. J. Appl. Phys.* **58**, SCCB28 (2019).

[20] A. Pesach, E. Gross, C.-Y. Huang, Y.-D. Lin, S. E. Schacham, S. Nakamura, and G. Bahir, *Appl. Phys. Lett.* **103**, 022110 (2013)

[21] J. Shao, D. Zakharov, C. Edmunds, O. Malis and M. J. Manfra, *Appl. Phys. Lett.* **103**, 232103 (2013).

[22] J. Shao, L. Tang, C. Edmunds, G. Gardner, O. Malis, and M. Manfra, *J. Appl. Phys.* **114**, 023508 (2013)

[23] T. Nguyen, M. Shirazi-HD, Y. Cao, R. E. Diaz, G. C. Gardner, M. Manfra, and O. Malis, *Phys. Status Solidi (a)* **215**, 1700828 (2018).

[24] M. Shirazi-HD, R. E Diaz, T. Nguyen, J. Jian, G. C. Gardner, H. Wang, M. J. Manfra, and O. Malis, *J. Appl. Phys.* **123**, 161581 (2018).

[25] A. Senichev, T. Nguyen, R. E Diaz, B. Dzuba, M. Shirazi-HD, Y. Cao, M. J. Manfra, and O. Malis, *APL Mater.* **7**, 121109 (2019).

[26] M. Sawicka, A. Feduniewicz-Żmuda, M. Kryśko, H. Turski, G. Muziol, M. Siekacz, P. Wolny, C. Skierbiszewski, *J. Cryst. Growth.* **459**, 129-134 (2017)

[27] R. Oliva, S. J. Zelewski, L. Janicki, K. R. Gwozdz, J. Serafinczuk, M. Rudzinski, E. zbay, and R. Kudrawiec, *Semicon. Sci. Technol.* **33**, 035007 (2018).

[28] I. Vurgaftman and J. R. Meyer, *J. Appl. Phys.* **94**, 3675-3696 (2003).

[29] Y. P. Varshni, *Physica.* **34**, 149-154 (1967).

[30] S. Birner, T. Zibold, T. Andlauer, T. Kubis, M. Sabathil, A. Trellakis, and P. Vogl, *IEEE Trans. Electron. Devices* **54**, 2137 (2007).

[31] U. M. E. Christmas, A. D. Andreev, and D. A. Faux, *J. Appl. Phys.* **98**, 073522 (2005).

[32] D. S. Arteev, A. V. Sakharov, E. E. Zavarin, W. V. Lundin, A. N. Smirnov, V. Y. Davydov, M. A. Yagovkina, S. O. Usov, and A. F. Tsatsulnikov, *J. Phys.: Conference Series.* **1135**, 012050 (2018).

[33] E. F. Schubert, E. O. Goebel, Y. Horikoshi, K. Ploog, and H. J. Queisser, *Phys. Rev. B.* **30**, 813-820 (1984).

[34] W. Shan, W. Walukiewicz, E. E. Haller, B. D. Little, J. J. Song, M. D. McCluskey, N. M. Johnson, Z. C. Feng, M. Schurman, and R. A. Stall, *J. Appl. Phys.* **84**, 4452-4458 (1998).

[35] C. Zhao, R. Zhang, B. Liu, D. Fu, H. Chen, M. Li, Z. Xie, X. Xiu, S. Gu, and Y. Zheng, *Science China Physics, Mechanics and Astronomy* **55**, 396-399 (2012).

[36] H. Wang, Z. Ji, S. Qu, G. Wang, Y. Jiang, B. Liu, X. Xu, and H. Mino, *Optics Express*. **20**, 3932-3940 (2012).

[37] Sh. F. Chichibu, A. Uedono, T. Onuma, B. A. Haskell, A. Chakraborty, T. Koyama, P. T. Fini, S. Keller, S. P. DenBaars, J. S. Speck, U. K. Mishra, S. Nakamura, S. Yamaguchi, S. Kamiyama, H. Amano, I. Akasaki, J. Han, and T. Sota, *Nature Mater.* **5**, 810-816 (2006).

[38] Y. Cho, G. H. Gainer, A. J. Fischer, J. J. Song, S. Keller, U. K. Misra, and S. P. DenBaars, *Appl. Phys. Lett.* **73**, 1370 (1998).

[39] M. N. Fireman, B. Bonef, E. C. Young, N. Nookala, M. A. Belkin, and J. S. Speck, *J. Appl. Phys.* **122**, 075105 (2017).

[40] T. K. Uždavinys, D. L. Becerra, R. Ivanov, S. P. DenBaars, S. Nakamura, J. S. Speck, and S. Marcinkevičius, *Optical Materials Express.* **7**, 3116-3123 (2017).

[41] M. Zíková, A. Hospodková, J. Pangrác, T. Hubáček, J. Oswald, K. Kuldová, F. Hájek, G. Ledoux, C. Dujardin, *J. Cryst. Growth.* **506**, 8-13 (2019).

[42] T. R. Merritt, M. A. Meeker, B. A. Magill, G. A. Khodaparast, S. McGill, J. G. Tischler, S. G. Choi, and C. J. Palmstrøm*, J. Appl. Phys.* **115**, 193503 (2014).

[43] Y. Huang, K. W. Sun, A. M. Fischer, Q. Y. Wei, R. Juday, F. A. Ponce, R. Kato, and T. Yokogawa, *Appl. Phys. Lett.* **98**, 261914 (2011).

[44] V. Liuolia, S. Marcinkevičius, Y.-D. Lin, H. Ohta, S. P. DenBaars, and S. Nakamura, *J. Appl. Phys.* **108**, 023101 (2010).

[45] S. Marcinkevičius, K. M. Kelchner, S. Nakamura, S. P. DenBaars, and J. S. Speck, *Appl. Phys. Lett.* **102**, 101102 (2013).

[46] C. Mounir, U. T. Schwarz, I. L. Koslow, M. Kneissl, and T. Wernicke, *Phys. Rev. B* **93**, 235314 (2016).

[47] R. Ivanov, S. Marcinkevicius, M. D. Mensi, O. Martinez, L. Y. Kuritzky, D. J. Myers, S. Nakamura, and J. S. Speck, *Phys. Rev. Appl.* **7**, 064033 (2017).

[48] R. Butte, L. Lahourcade, T. K. Uzdavinys, G. Callsen, M. Mensi, M. Glauser, G. Rossbach, D. Martin, J.-F. Carlin, S. Marcinkevicius, and N. Grandjean, *Appl. Phys. Lett.* **112**, 032106 (2018).

[49] Ž. Podlipskas, J. Jurkevičius, A. Kadys, S. Miasojedovas, T. Malinauskas, and R. Aleksiejūnas, *Sci. Rep.* **9**, 17346 (2019).

[50] Y. Xing, L. Wang, D. Yang, Z. Wang, Z. Hao, C. Sun, B. Xiong, Y. Luo, Y. Han, J. Wang and H. Li, *Sci. Rep.* **7**, 45082 (2017).

[51] M. Pophristic, F. H. Long, C. Tran, I. T. Ferguson and R. F. Karlicek, Jr., *J. Appl. Phys.* **86**, 1114 (1999).

[52] S. Marcinkevičius, K. M. Kelchner, L. Y. Kuritzky, S. Nakamura, S. P. DenBaars, and J. S. Speck, *Appl. Phys. Lett.* **103**, 111107 (2013).